

SINGLE IMAGE DEFOCUS MAP ESTIMATION USING LOCAL CONTRAST PRIOR

Yu-Wing Tai[‡], Michael S. Brown[†]

Korea Advanced Institute of Science and Technology[‡]
National University of Singapore[†]

ABSTRACT

Image defocus estimation is useful for several applications including deblurring, blur magnification, measuring image quality, and depth of field segmentation. In this paper, we present a simple yet effective approach for estimating a defocus blur map based on the relationship of the contrast to the image gradient in a local image region. We call this relationship the local contrast prior. The advantage of our approach is that it does not require filter banks or frequency decomposition of the input image; instead we only need to compare local gradient profiles with the local contrast. We discuss the idea behind the local contrast prior and demonstrate its effectiveness on a variety of experiments.

1. INTRODUCTION

We present a method to estimate the defocus map in an image using the *local contrast prior*. The local contrast prior considers the relationship of local image gradients to local image contrast as shown in Fig. 1. For image regions that exhibit defocus blur, the magnitude of image gradients within that region are smaller than the local contrast due to the smoothing effect of the blurring process. The larger the defocus blur, the larger this difference between the magnitude of the image gradient to local contrast. Thus by computing this ratio of maximum gradient to the local image contrast, we obtain a simple, yet effective blur estimations that does not require filter-banks or frequency decomposition of the image.

In this paper, we describe a fully automated method based on the local contrast prior to estimate a defocus blur map. To overcome large homogenous regions where the local contrast prior cannot be defined, we describe a Markov Random Field (MRF) formulation to propagate local estimation to generate a full image defocus map.

Our paper is organized as follows: section 2 provides a background and discussion of related work on image defocus and its estimation; section 3 discusses the local contrast prior and its characteristics in natural images; section 4 demonstrates our approach on a variety of examples and demonstrate its use on applications such as image deblurring, depth of field segmentation, and image quality measurement; the paper is concluded in section 5.

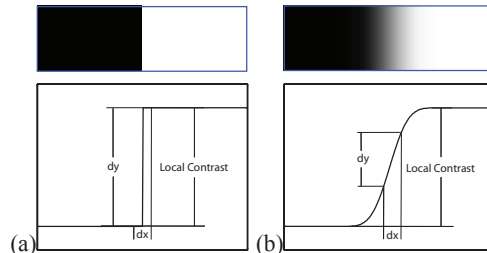


Fig. 1. The relationship between local image gradient and local image contrast. A sharp edge in (a) undergoes defocus blur in (b). Inside the same neighborhood, the image contrast is invariant to the defocus blur while image gradient strictly decreasing.

2. BACKGROUND AND RELATED WORK

2.1. Image Defocus

The two principal causes of image defocus are limited depth of field (DOF) and lens aberrations that cause light rays to converge incorrectly onto the imaging sensor. Defocus of the first type is illustrated by the point q in Fig. 2 and is described by the thin lens law [2]:

$$\frac{1}{S_1} + \frac{1}{f_1} = \frac{1}{f}, \quad (1)$$

where f is the focal length of the lens, S_1 is the distance of the focal plane in the scene from the lens plane, and f_1 is the distance from the lens plane to the sensor plane.

The blurred spot caused by limited DOF or lens aberrations is called the circle of confusion. From Eq. (1) and the relationship of parameters in Fig. 2, the diameter of circle of confusion is:

$$C = A \cdot \frac{|S_2 - S_1|}{S_2} \cdot \frac{f}{|S_1 - f|}, \quad (2)$$

which concurs that the diameter C increases as the distance of a point from the focal plane $|S_2 - S_1|$ increases and C decreases as the aperture diameter A decreases. For defocus blur caused by lens aberrations, C increases as the distance $|r - p|$ increases.

Depending on the shape and diffraction of the aperture, the circle of confusion is not strictly a circle. The intensity within the circle of confusion can be assumed to be uniform [16]. However, if the effects of diffraction and the lens system are taken into account, the intensity within the blur

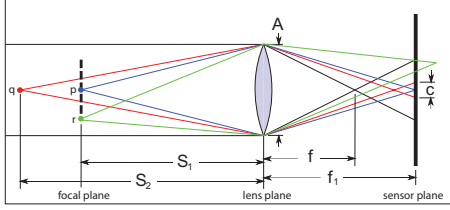


Fig. 2. Optical geometry for different causes of defocus blur. Point q : Defocus due to limited depth of field. Point r : Defocus due to lens aberrations.

circle can be reasonably approximated by a Gaussian distribution [14, 4, 10]. Thus, the defocus blur effect can be formulated as the following convolution:

$$I_{ob} = I \otimes h + n, \quad (3)$$

where I_{ob} is the observed image, I represents an in-focus image of the scene, h is a spatially-varying Gaussian blur kernel, and n denotes additive noise. Under this configurations, the estimation of h for each image pixel is equal to the estimation of a defocus blur scale map (i.e. defocus map).

2.2. Related Work

Our work is related to blur/defocus estimation from a single image. Previous work on blur estimation from a single image include Elder and Zucker [3] that proposed to model focal blur by a Gaussian blur kernel. This work used the first and second order derivative from steerable Gaussian basis filters to calculate the center line of edges and blur responses. Saxena *et al* [15] proposed a supervised learning approach to estimate a defocus map by comparing the filter responses of image patches to the responses from training data. Bae and Durand [1] extended the work in [3] with an MRF and cross bilateral filtering to maintain smoothness and reduce estimation errors. Levin *et al* [12] proposed to use a coded aperture in the image capture process to aid defocus estimation. Liu *et al* [13] proposed to use multiple features that included the local power spectrum slope in the frequency domain, gradient histogram span, color saturation and local autocorrelation congruency for blur detection and classification. Blur estimation is also related to image segmentation used to segment regions of interest from DOF images. Wang *et al* [17] used wavelet coefficients to identify regions with high frequency details. Kim [7] segmented in-focus regions from DOF image using high-frequency components with morphological filters to fill holes. Kovács and Szirányi [9] identify in-focus regions based on blind deconvolution algorithm. These previous approaches, however, all require either filter banks or frequency decomposition in the estimation process. Our work is unique in that we do not require filter banks or frequency decomposition, but instead only need to consider local image gradients and contrast which is a much simpler technique compared with previous approaches.

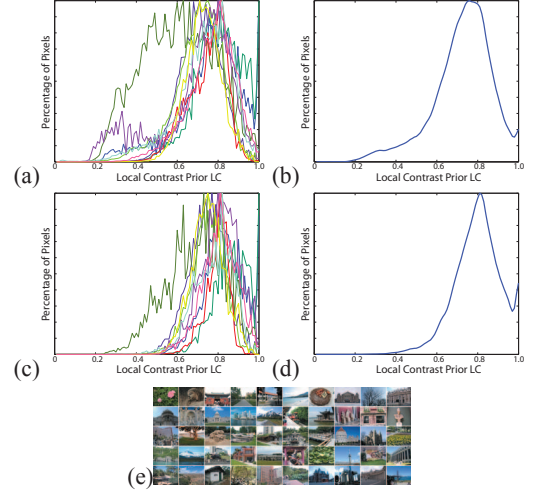


Fig. 3. The distribution of the local contrast prior in high quality natural in-focus images. (a) We plot the the distributions of LC of 10 images randomly selected from our samples. (b) Estimated distribution of (a) using GMM. (c) The edge pixels' distributions of LC of the 10 selected images. Edge pixels are defined by using a canny edge detector. (d) Estimated distribution of (c) using GMM. (e) 50 images from our samples.

3. THE LOCAL CONTRAST PRIOR

Recent studies [11, 5] have shown that the marginal distribution of image gradients follow a similar characteristic among natural images. The so called *natural image statistics prior* is powerful in image analysis and as a regularization term for image deblurring [11, 5]. In [6], Sun *et al* studied the *gradient profile prior* and found that the edge sharpness of natural images follows a certain distribution which is independent of image resolution. The gradient profile prior was applied to single image super-resolution in [6]. This paper follows this trend by first showing the characteristics on the distribution of the local contrast prior in natural images. We then discuss how to convert local contrast prior measurements into a defocus map using MRF propagation and its applications in the experimental section 4.

3.1. Distribution of Local Contrast Prior in Natural Images

The relationship we want to study is defined as follow:

$$LC(x, y) = \frac{\max |\nabla I(x', y')|}{\max I(x', y') - \min I(x', y')}, \quad (4)$$

where $(x', y') \in \mathcal{N}(x, y)$ is the neighborhood of (x, y) . If (x, y) is inside a homogeneous or smooth region, e.g. $\max I(x', y') - \min I(x', y') < t$, we consider $LC(x, y)$ to be undefined. In our implementation, we set $\mathcal{N}(x, y)$ to be a local window of size 11×11 and $t = 25$ with respect to the intensity range from 0 to 255. Unlike natural image statistics our measurement is computed locally. If pixels have small

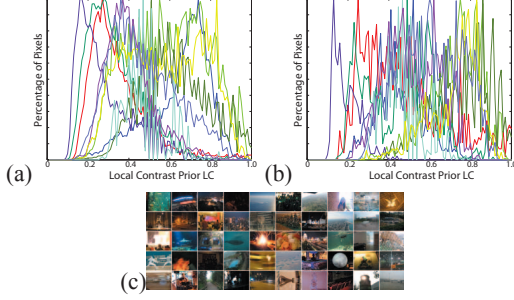


Fig. 4. The distribution of the local contrast prior in low quality images. (a) The distributions of LC of 10 images randomly selected from our samples. (b) The edge pixels’ distributions of LC of the 10 selected images. (c) 50 images from our samples.

image gradients and the local contrast is also small, $LC(x, y)$ gives a large value.

Fig. 3 shows a histogram of the local contrast prior (LC) defined in Eq.(4) from 50 natural in-focus images from professional photography forums. The x-axis is LC scores and y-axis is percentage of pixels. We normalized the histograms so that they have the same maximum value in the y-axis for better visualization and comparison. The distribution of LC peaks at around 0.8 in Fig. 3-(b) which represents the average sharpness of in-focus edge pixels. This plot agrees with the distribution in Fig. 3-(d) for which only edge pixels are included in the estimation. The small peak at 1.0 indicates the existence of step edges that usually exists in photos containing man-made structures such as buildings. Fig. 3-(b) and (d) decreases to zero gradually, but (b) has a longer tail as the result of soft edges caused by shadings, shadows, etc. We found that there are large image regions where LC is undefined. The undefined LC is from homogeneous regions which agrees with natural image statistics that most pixels will have zero or small gradient magnitudes.

To verify whether the distribution is uniquely defined for in-focus images, we collect another 50 low quality images that included images suffering from defocus blur, motion blur, noise, over exposures, etc, and plot their LC distribution. Fig. 4 shows 10 distributions randomly selected. As we can see from the Fig. 4-(a), the distribution of LC becomes more uniformly distributed with more weight at small values and less weight at $LC(x, y) = 1$. The peak of edge pixel distributions of the LC have shifted to left. The distribution of LC contains more than one peak for which peaks at small values are from out-of-focus regions and peaks at large values are from in-focus regions.

If an in-focus image contains an edge with $LC(x, y) = m$, after a convolution process caused by defocus blur, the expected gradient magnitude of $LC(x, y)$ should be approximately equal to $\frac{m}{\sqrt{2\pi}\sigma}$ if the circle of confusion follows a gaussian spherical kernel with standard derivation equal to σ . Hence, if an image is suffering from defocus blur, its aver-

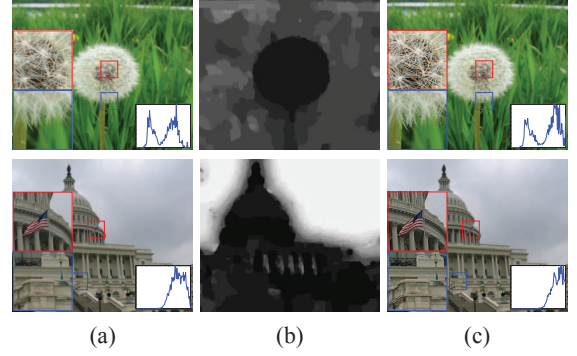


Fig. 5. Recover in-focus image from defocused image on other examples. (a) Input images, (b) our estimated defocus map, (c) recovered in-focus images. The distribution of edge pixels’ LC are also shown.

age LC will be smaller than an in-focus image. Based on the above observation, we can estimate the defocus scale (in terms of σ) by assuming the expected LC of edges is approximately equal to 0.8 (Fig. 3-(b)-(d)). In our implementation, we assume the defocus blur kernel is gaussian spherical kernel [14, 4, 10].

3.2. MRF Propagation

Estimating LC for each pixel is not robust due to the noise and existence of soft edges and potentially large homogenous regions. We use an MRF to refine our estimated defocus map. Since the LC is not linearly related to the defocus scale, we transform the LC into a defocus scale radius $R_{LC} = \frac{0.8/\sqrt{2\pi}}{LC}$ before our MRF propagation. R_{LC} is truncated to the range between $\mu_{R_{LC}} \pm 2\sigma_{R_{LC}}$, where $\mu_{R_{LC}}$ and $\sigma_{R_{LC}}$ are the mean and standard derivation of R_{LC} respectively. We quantize R_{LC} into discrete labels $\{\bar{R}_{LC}\}$, and we use first order neighborhood $N(\cdot)$ to build our Markov network. Our data term and pairwise energy term are defined as follows:

$$\sum_i [w_i(\bar{R}_{LC}(i) - R_{LC}(i))^2 + \alpha \sum_{j \in N(i)} w_{ij}(\bar{R}_{LC}(i) - \bar{R}_{LC}(j))^2] \quad (5)$$

where $w_i = \frac{\max I(x', y') - \min I(x', y')}{\max I(x, y) - \min I(x, y)}$ is a weight of measurement by comparing the local contrast to global contrast. High confidence is given to pixel with large local contrast since these pixel are less sensitive to noise and are more accurate about estimation of the LC . The term $w_{ij} = |I_i - I_j|^2$ is the color difference between neighborhood pixel which asserts that if the neighborhood pixel has similar color, they should have similar defocus scale. The term α is set to 1 in our implementation. The final defocus map is obtained using Graph cuts [8] to find the optimal \bar{R}_{LC}^* that minimize Eq. (5).

4. EXPERIMENTS

Fig. 5 show our results for estimating defocus maps. We use the estimated defocus map to enhance the quality of the images through deconvolution. After enhancement we see that the edge pixels LC ’s distribution shift’s slightly to the right

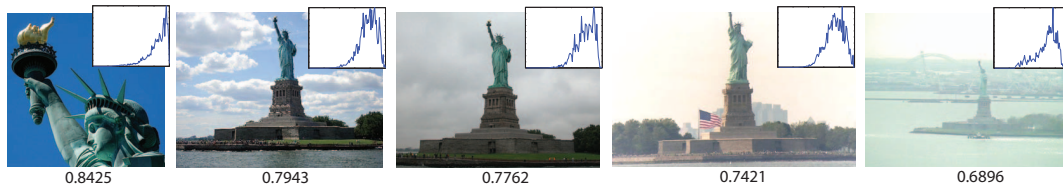


Fig. 6. Quality Ranking. We rank the quality of images according to the mean value (below each image) of edge pixels' LC . The larger value meaning that the image contains more sharp edges which considered to have higher quality. The distribution of edge pixels' LC are also shown.



Fig. 7. Region Of Interest Extraction. The Local Contrast Prior can also be used to extract in-focus regions from depth of field images. The first row show depth of field images, the second row show the extracted in-focus regions.

denoting an increase in stronger image gradients in the enhanced image.

The local contrast prior can also be used to segment in-focus regions from depth-of-field images. After MRF propagation, we calculate the average defocus scale within each label. A pixel is assigned to be in-focus if the average LC of the pixel label is larger than 0.75. Fig. 7 shows our segmentation results. Note that the images we tested contain similar color and texture in both in-focus region and out-of-focus regions. Our approach is successful in segmenting the in-focus region from depth-of-field images.

Fig. 6 shows an example to use the local contrast prior for ranking image quality. We rank the quality of images according to the mean of edge pixels' LC . The distribution of edge pixels' LC are also shown in Fig. 6. Our quality ranking agrees with human ranking about the image quality of the 5 images.

5. CONCLUSIONS AND DISCUSSIONS

In this paper, we proposed the local contrast prior (LC), a simple and effective measurement of defocus blur. We found that for natural in-focus images, this distribution follows a similar pattern as shown in Fig. 3. We verified this distribution by plotting the distribution of the LC in images suffered from different type of degradation as shown in Fig. 4. This prior is useful in estimating defocus blur, in segmenting in-focus regions from depth-of-field image and in ranking image quality. In future work, we plan to study the properties of the distribution of the local contrast prior under different degree of blurriness/noise and to investigate the possibility of using the local contrast prior in other applications.

6. ACKNOWLEDGEMENTS

This work was supported in part by a Singapore AcRF Tier-1 grant (Project No. R-252-000-333-133) and by a KAIST seed grant.

7. REFERENCES

- [1] S. Bae and F. Durand. Defocus magnification. *Comput. Graph. Forum*, 26(3):571–579, 2007.
- [2] M. Born and E. Wolf. *Principles of Optics*. Cambridge Univ. Press, seventh edition, 1999.
- [3] J. H. Elder and S. W. Zucker. Local scale control for edge detection and blur estimation. *IEEE Trans. PAMI*, 20(7):699–716, 1998.
- [4] P. Favaro and S. Soatto. A geometric approach to shape from defocus. *IEEE Trans. PAMI*, 27(3):406–417, 2005.
- [5] R. Fergus, B. Singh, A. Hertzmann, S. T. Roweis, and W. T. Freeman. Removing camera shake from a single photograph. *ACM Trans. Graphics*, 25(3):787–794, 2006.
- [6] J. Sun, J. Sun, Z. Xu, and H. Shum. Image super-resolution using gradient profile prior. In *CVPR*, 2008.
- [7] C. Kim. Segmenting a low-depth-of-field image using morphological filters and region merging. *IEEE TIP*, 14(10):1503–1511.
- [8] V. Kolmogorov and R. Zabih. What energy functions can be minimized via graph cuts? *IEEE Trans. PAMI*, 26(2):147–159, 2004.
- [9] L. Kovács and S. Szirányi. Focus area extraction by blind deconvolution for defining regions of interest. *IEEE Trans. PAMI*, 29(6):1080–1085, 2002.
- [10] A. Kubota and K. Aizawa. Reconstructing arbitrarily focused images from two differently focused images using linear filters. *IEEE TIP*, 14(11):1848–1859, 2005.
- [11] A. Levin. Blind motion deblurring using image statistics. In *NIPS*, 2006.
- [12] A. Levin, R. Fergus, F. Durand, and W. T. Freeman. Image and depth from a conventional camera with a coded aperture. *ACM Trans. Graphics*, 2007.
- [13] R. Liu, Z. Li, and J. Jia. Image partial blur detection and classification. In *CVPR*, 2008.
- [14] T. Sakamoto. Model for spherical aberration in a single radial gradient-rod lens. *Applied Optics*, 23(11):1707–1710, 1984.
- [15] A. Saxena, S. H. Chung, and A. Y. Ng. Learning depth from single monocular images. In *NIPS*, 2005.
- [16] M. Subbarao and N. Gurumoorthy. Depth recovery from blurred edge. In *CVPR*, pages 498–503, 1988.
- [17] J. Z. Wang, J. Li, R. Gary, and G. Wiederhold. Unsupervised multisolution segmentation for images with low depth of field. *IEEE Trans. PAMI*, 23(1), 2001.